

Q-balls without a potential

V. Loiko^{*}, I. Perapechka^{*} and Ya. Shnir[†]

^{*}*Department of Theoretical Physics and Astrophysics,*

Belarusian State University, Minsk 220004, Belarus

[†]*BLTP, JINR, Dubna 141980, Moscow Region, Russia*

We study non-topological Q-ball solutions of the (3+1)-dimensional Friedberg-Lee-Sirlin two-component model. The limiting case of vanishing potential term yields an example of hairy Q-balls, which possess a long range massless real field. We discuss the properties of these stationary field configurations and determine their domain of existence. Considering Friedberg-Lee-Sirlin model we present numerical evidence for the existence of spinning axially symmetric Q-balls with different parity. Solution of this type exist also in the limiting case of vanishing scalar potential. We find that the hairy Q-balls are classically stable for all range of values of angular frequency.

I. INTRODUCTION

Q-balls are stationary non-topological solitons, which may exist in a model with complex scalar fields. Configurations of this type were introduced in 1976 by Friedberg, Lee and Sirlin in two-component model with symmetry breaking potential [1], a few years later Coleman found another realization of Q-balls considering a single complex scalar field in a model with a non-renormalizable self-interaction potential [2]. In both cases the global phase invariance of the scalar field is associated with a conserved $U(1)$ Noether charge Q , the Q-balls correspond to stationary points of the total energy functional for a given value of the charge.

Q-balls attracted a lot of attention because it was suggested that such configuration may contribute to various scenario of the evolution of the early Universe [3–5]. The Q-balls also can occur in the minimal supersymmetric generalization of the Standard Model, where one finds leptonic and baryonic Q-balls related with conservation of lepton and baryon number, respectively [6]. Further, it was argued that these Q-balls may play an essential role in baryogenesis via the Affleck-Dine mechanism [7], they also were considered as candidates for dark matter [8]. Q-balls may exist in a wide variety of physical systems. Solutions of that

type were constructed in Abelian gauge models with local $U(1)$ symmetry [9, 10], in non-Abelian gauge theories [1, 11, 12] and other models. An interesting realization of the Q-balls exists in condensed matter systems where they appear in the Bose-Einstein condensate [13], or in the superfluid $^3\text{He-B}$ [14].

Spherically symmetric Q-balls exist only within a certain angular frequency range, which is determined by the explicit structure of the potential. Notably, in the Friedberg-Lee-Sirlin model, which describes dynamics of a real self-interacting scalar field, coupled to a complex scalar field, the lower critical frequency is zero. Typically, there are two branches of Q-ball solutions, which are represented by two curves of the dependencies of the energy of the configuration on its charge [1]. Solutions are stable along the lower branch, when their mass is smaller than the mass of free charged quanta of scalar excitations. In the simplest case the Q-balls are spherically symmetric, however there are generalized spinning axially symmetric solutions with non-zero angular momentum [16, 17]. The energy density of these spinning Q-balls is of toroidal shape.

There are some important differences between the Q-ball solutions of the Coleman model [2] with a single complex field and sextic potential, and the corresponding solutions of the renormalizable Friedberg-Lee-Sirlin model [1]. An interesting feature of Q-balls in the Friedberg-Lee-Sirlin model is that in 3+1 dimensions these localized configurations with finite energy may also exist in the limiting case of vanishing scalar potential [15]. It was pointed out that in such a limit the Q-balls are stabilized by the gradient terms in the energy functional. Further, the corresponding real scalar component becomes massless, it possess Coulomb-like asymptotic tail.

However, the paper [15] contains only qualitative discussion of the corresponding solutions, they were not constructed explicitly, further the authors do not study the frequency dependence of these solitons and their stability.

The main purpose of this work is to construct explicit examples of stationary solutions of the Friedberg-Lee-Sirlin model in the limit of vanishing potential that have not been studied so far, fully investigate properties of these Q-balls and determine their domains of existence. We also consider spinning configurations with non-zero angular momentum with both even and odd parity and address the issue of classical stability of these solutions.

II. SPHERICALLY SYMMETRIC SOLUTIONS

The 3+1 dimensional Friedberg-Lee-Sirlin model describes a real self-interacting scalar field ξ , coupled to a complex scalar field ϕ :

$$L = (\partial_\mu \xi)^2 + |\partial_\mu \phi|^2 - m^2 \xi^2 |\phi|^2 - U(\xi), \quad (1)$$

where κ is the coupling constant. The potential of the real scalar field is

$$U(\xi) = \mu^2(1 - \xi^2)^2, \quad (2)$$

thus, $\xi \rightarrow 1$ in the vacuum and the complex field ϕ becomes massive due to the coupling with its real partner. Thus, the parameters μ and m corresponds to the mass of the real and complex components, respectively.

Similar to the Coleman model with a non-renormalizable sextic potential [2], the model (1) is invariant under the global $U(1)$ transformations of the complex field $\phi \rightarrow \phi e^{i\alpha}$. The Noether current, associated with this symmetry, is

$$j_\mu = i(\phi \partial_\mu \phi^* - \phi^* \partial_\mu \phi); \quad \partial^\mu j_\mu = 0, \quad (3)$$

and the conserved charge is

$$Q = i \int d^3x (\phi \partial_t \phi^* - \phi^* \partial_t \phi). \quad (4)$$

First, we consider the usual spherically symmetric parametrization of the fields

$$\xi = X(r); \quad \phi = Y(r)e^{i\omega t}, \quad (5)$$

where $X(r)$ and $Y(r)$ are real functions of radial variable and ω is the frequency of stationary rotation.

Substitution of this ansatz into the stationary energy functional gives

$$E = \int d^3x T_0^0 = 4\pi \int_0^\infty dr r^2 \left[\left(\frac{dX}{dr} \right)^2 + \left(\frac{dY}{dr} \right)^2 + \omega^2 Y^2 + \mu^2(1 - X^2)^2 + m^2 Y^2 X^2 \right], \quad (6)$$

and the charge of the spherically symmetric Q-ball is

$$Q = 8\pi\omega \int_0^\infty dr r^2 Y^2. \quad (7)$$

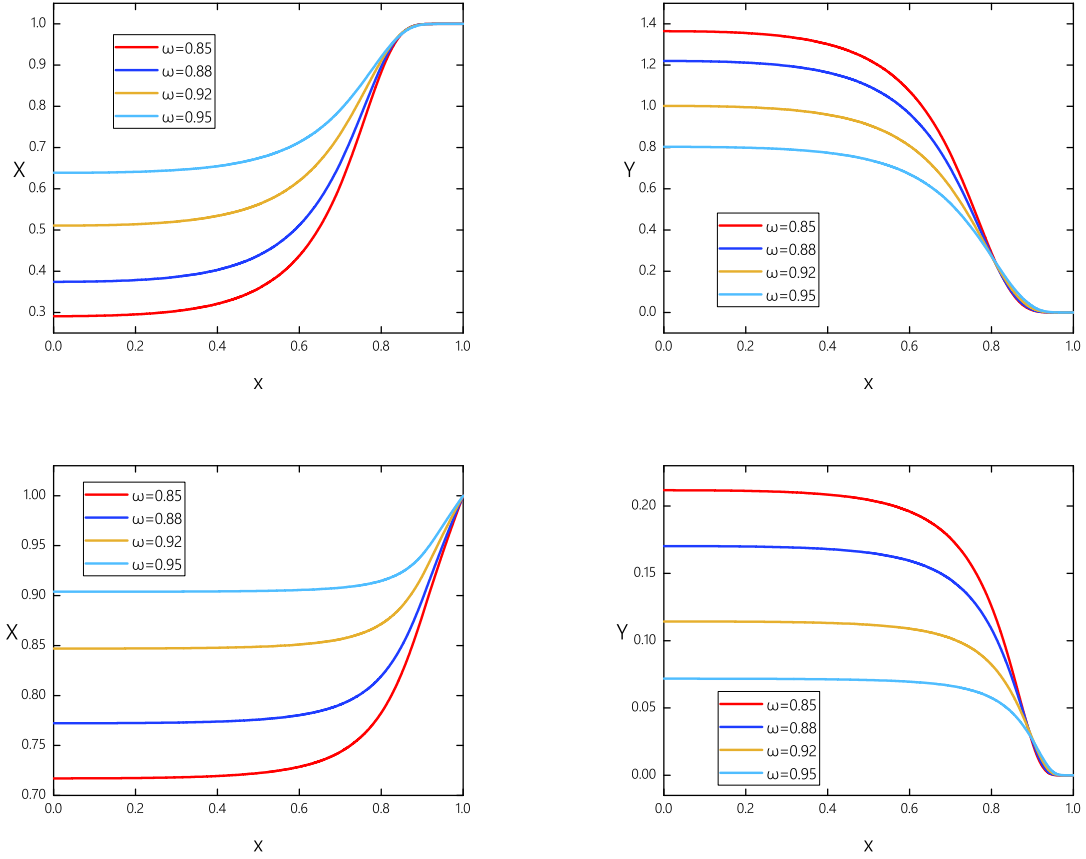


FIG. 1: The profiles of the field components of the Friedberg–Lee–Sirlin Q-ball configuration are plotted as functions of the compact radial variable $x = r/(1+r)$ for some set of values of angular frequency ω at $m = 1$ and $\mu^2 = 0.25$ (upper plots) and $\mu^2 = 0$ (bottom plots).

The field equations of the model become

$$\begin{aligned} \frac{d^2 X}{dr^2} + \frac{2}{r} \frac{dX}{dr} + 2\mu^2 X(1 - X^2) - m^2 XY^2 &= 0; \\ \frac{d^2 Y}{dr^2} + \frac{2}{r} \frac{dY}{dr} + \omega^2 Y - m^2 X^2 Y &= 0. \end{aligned} \quad (8)$$

Like other Q-ball dynamical equations [1, 16, 18–20], this system effectively describes a unit mass pseudo-particle moving in two dimensional plane parameterized by the "coordinates" $X(r), Y(r)$ and "time" r , in direction Y in the effective potential

$$U_{eff} = \omega^2 Y^2 - \mu^2(1 - X^2)^2 - m^2 Y^2 X^2 \quad (9)$$

Non-topological soliton solution may exist when the trivial configuration $X = Y = 0$ corresponds to a local maximum of the effective potential. This restriction corresponds to

the upper bound on the angular frequency $\omega_+ = m$, the Q-ball continuously approaches perturbative solutions as ω approaches this critical value [1]. Thus, the upper bound of the angular frequency of the Q-ball corresponds to the mass of the complex component m , the localized soliton configuration with finite energy may exist as its real component $X(r)$ becomes massless [15]. Hereafter we fix $m = 1$, without loss of generality. Note that, unlike the Q-balls in the non-renormalizable model with single complex field and sextic potential [2], there is no lower bound on the frequency, the solutions of the model (1) exists for all non-zero values of the angular frequency ω . As ω decreases, the characteristic size of the configuration is increasing.

The vacuum boundary conditions on the spacial infinity are $X \rightarrow 1$, $Y \rightarrow 0$ as $r \rightarrow \infty$ and the condition of regularity at the origin is

$$\frac{dX}{dr} = \frac{dY}{dr} = 0, \quad \text{as } r \rightarrow 0.$$

Imposing the boundary conditions we can find numerical solutions of the system of coupled ordinary differential equations (8). In our calculations we used the usual shooting algorithm, based on Dormand-Prince 8th order method with adaptive stepsize. The relative errors of calculations are lower than 10^{-10} .

In Fig. 1 we displayed the corresponding solutions at $m = 1$ and $\mu^2 = 0.25$. The parameter μ yields the mass of the excitations of the real component X , it approaches the vacuum asymptotic value as $X \sim 1 - e^{-\sqrt{\mu^2 - \omega^2} r}$. Setting $\mu = 0$ changes the asymptotic behavior, in such a case the real massless field $X(r)$ decays as [15]

$$X(r) \sim 1 - \frac{C}{r} + O(r^{-2}) \quad \text{as } r \rightarrow \infty \quad (10)$$

This is a long-range Coulomb asymptotic with a scalar charge C , see Fig. 1, bottom plots.

The charge and the energy of the Q-balls are given by (6),(7), respectively. As the mass of the real component remains non-zero, the curves of dependency of both the charge and the mass on the angular frequency exhibit the typical two-branch behavior, see Fig. 2, left plot. At some critical value of the frequency ω_{cr} the energy and the charge of the configuration are taking minimal non-zero values, they diverge as ω approaches the upper bound, and in the opposite limit, as ω decreases to zero. Decrease of the mass parameter μ for a fixed value of the frequency ω yields decrease of both the energy and the charge of the Q-ball. Fig. 3 exhibits the $E(Q)$ curves of the configurations at $\mu^2 = 0.25$ and in the massless case $\mu = 0$.

In Fig. 3 we also indicate the energy of Q free scalar quanta $E = mQ$, this is a straight line separating the stability region, the configuration is classically stable below this line.

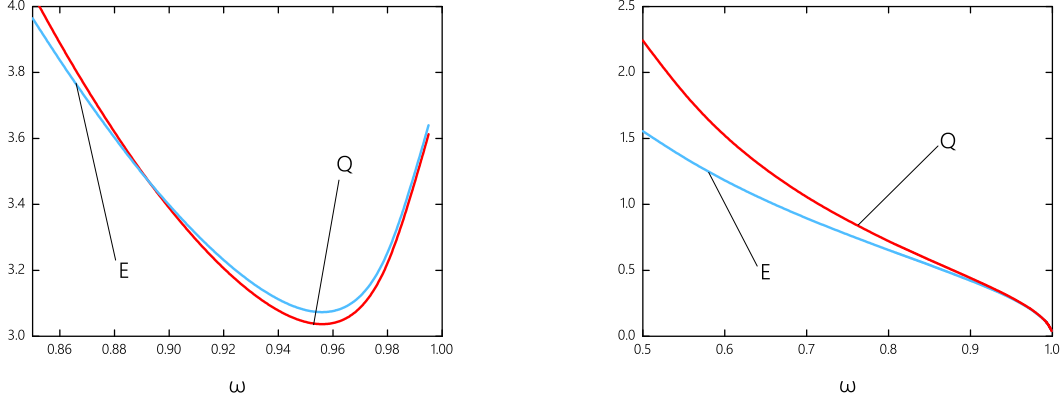


FIG. 2: The energy and the charge of the spherically symmetric Q-balls are shown in units of 16π as functions of the angular frequency ω at $m = 1$, $\mu^2 = 0.25$ (left) and $\mu^2 = 0$ (right).

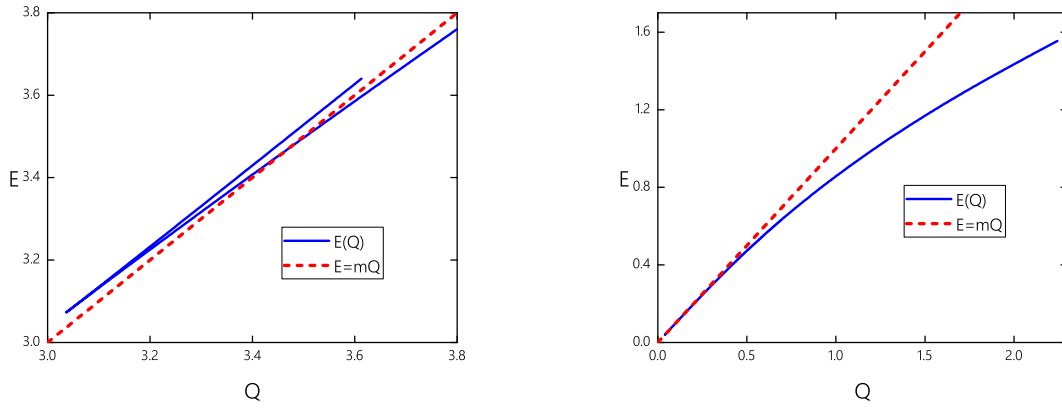


FIG. 3: The energy of the spherically symmetric Q-balls is plotted as a function of the charge Q at $m = 1$, $\mu^2 = 0.25$ (left) and $\mu^2 = 0$ (right). The straight line $E = mQ$ indicates the boundary of the stability region.

Indeed, for $\mu \neq 0$, there are two branches of $E(Q)$ curves with a sharp cusp at $\omega = \omega_{cr}$ (see Fig. 3, left plot). The lower in energy branch corresponds to the values of the frequency $\omega < \omega_{cr}$ whereas the upper branch corresponds to $\omega > \omega_{cr}$. As the real component remains massive, the configurations on the upper branch are unstable [1]. We observe that decrease of the mass parameter μ shifts the critical value ω_{cr} towards the upper limit ω_+ .

The situation changes dramatically in the massless limit $\mu = 0$, the stable branch extends all the way up to the critical value $\omega_+ = m$, here both components of the Q-ball approach the corresponding vacuum values and both the energy and the charge of the configuration tend to zero, see Fig. 2. Thus, the hairy Q-balls with long-range real scalar component are classically stable for all range of values of the angular frequency.

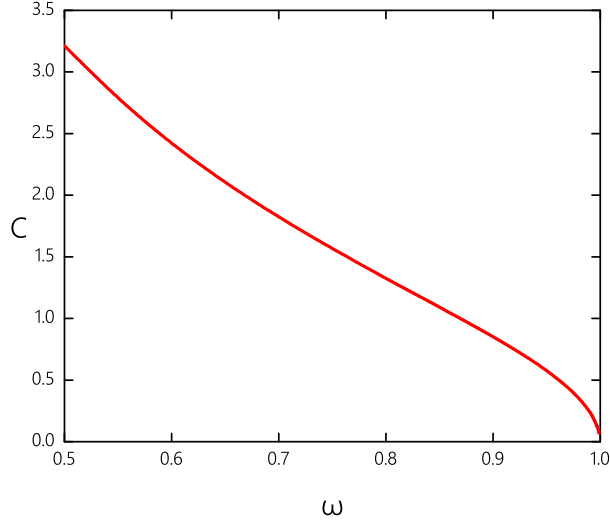


FIG. 4: The scalar charge of the Q-balls with massless component X is plotted as a function of the frequency ω .

Note that the scalar charge C , which corresponds to the Coulomb asymptotic tail of the hairy Q-ball (10), is not a constant. The configuration is not rigid, its characteristic size varies with the angular frequency ω . Indeed, numerical calculations show that the value of the charge C monotonically decreases, as ω increases, see Fig. 4. However, the relation $C = \sqrt{Q/2}$, which follows from some qualitative arguments [15], holds only for large Q-balls, i.e. for small values of the angular frequency ω .

III. SPINNING SOLUTIONS

A generalization of the fundamental spherically symmetric Q-ball can be constructed when we consider spinning axially symmetric configuration [16, 17]:

$$\xi = X(r, \theta); \quad \phi = Y(r, \theta)e^{i(\omega t + n\varphi)}, \quad (11)$$

which generalizes the ansatz (5). Here $n \in \mathbb{Z}$ is a rotational quantum number, the angular momentum of the stationary spinning Q-ball is classically quantized as [16]

$$J = \int d^3x T_\varphi^0 = 4\pi n\omega \int_0^\infty \int_0^\pi dr d\theta \sin\theta r^2 Y^2 = nQ. \quad (12)$$

The real functions $X(r, \theta), Y(r, \theta)$ depend on the polar angle θ and radial variable r . The energy of the configuration then read

$$E = 2\pi \int_0^\pi \int_0^\infty \sin\theta r^2 dr d\theta \left[X_r^2 + Y_r^2 + \frac{X_\theta^2}{r^2} + \frac{Y_\theta^2}{r^2} + \left(\omega^2 + \frac{n^2}{r^2 \sin^2\theta} \right) Y^2 + \mu^2(1 - X^2)^2 + m^2 Y^2 X^2 \right]. \quad (13)$$

The corresponding field equations are

$$\begin{aligned} \left(\frac{\partial^2}{\partial r^2} + \frac{2}{r} \frac{\partial}{\partial r} + \frac{1}{r^2} \frac{\partial^2}{\partial \theta^2} + \frac{\cos\theta}{r^2 \sin\theta} \frac{\partial}{\partial \theta} + 2\mu^2(1 - X^2) - m^2 Y^2 \right) X &= 0 \\ \left(\frac{\partial^2}{\partial r^2} + \frac{2}{r} \frac{\partial}{\partial r} + \frac{1}{r^2} \frac{\partial^2}{\partial \theta^2} + \frac{\cos\theta}{r^2 \sin\theta} \frac{\partial}{\partial \theta} - m^2 X^2 + \omega^2 - \frac{n^2}{r^2 \sin^2\theta} \right) Y &= 0 \end{aligned} \quad (14)$$

Note that these equations are symmetric with respect to reflections in the $\theta = \pi/2$ plane.

To find numerical solutions of these coupled partial differential equations we used the software package CADSOL based on the Newton-Raphson algorithm [21]. The numerical calculations are mainly performed on an equidistant grid in spherical coordinates r and θ . Typical grids we used have sizes 70×60 . As before, we map the infinite interval of the variable r onto the compact radial coordinate $x = \frac{r/r_0}{1+r/r_0} \in [0 : 1]$. Here r_0 is a real scaling constant, which typically is taken as $r_0 = 4 - 6$. For spinning Q-balls the component $Y(r, \theta)$ must vanish at the origin, both in the massive and in the massless cases. The restriction of regularity also yields $\partial_r X(r, \theta) = 0$ as $r \rightarrow 0$.

To secure the condition of regularity on the symmetry axis we impose there the boundary conditions

$$\partial_\theta X|_{\theta=0,\pi} = 0, \quad Y|_{\theta=0,\pi} = 0. \quad (15)$$

The spinning Q-balls correspond to stationary points of the action functional, they exist only for a restricted frequency range. Previously they have been constructed only for the model with a single complex field and sextic potential [16, 17]. A peculiar feature of these Q-balls is that for a non-zero rotational quantum number n there are two different solutions

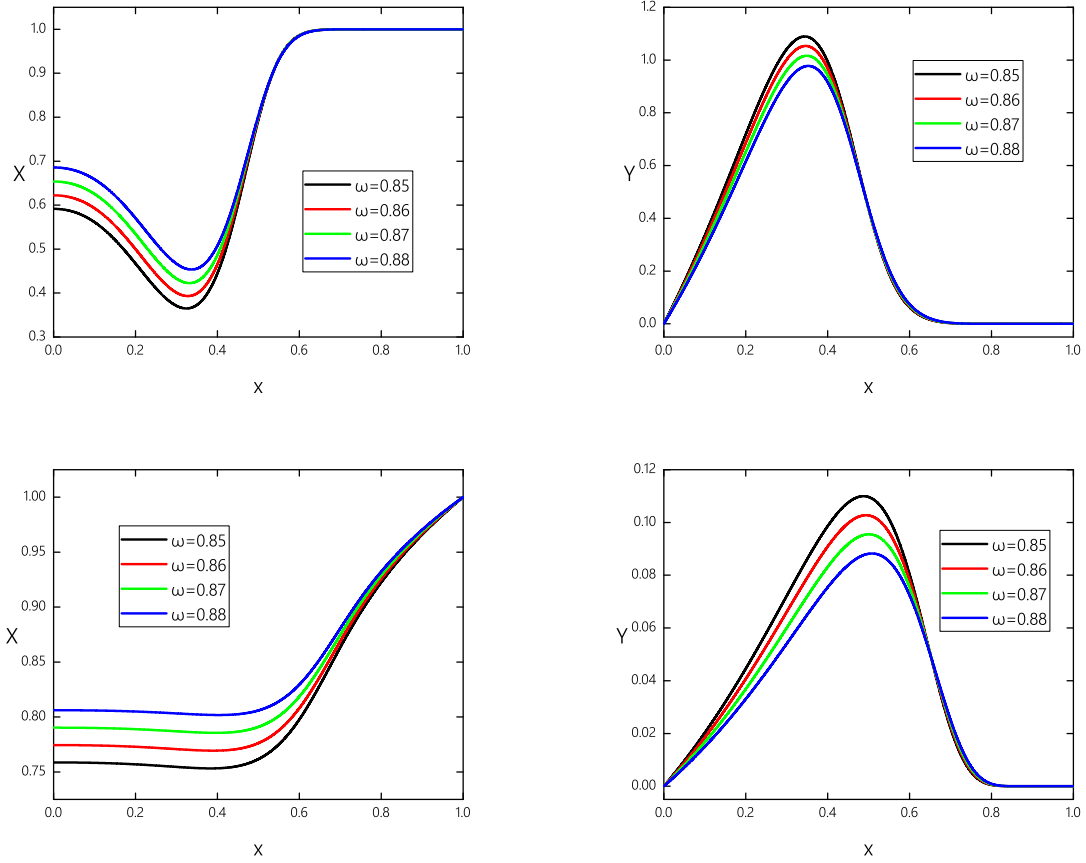


FIG. 5: The profiles of the field components of the spinning $n = 1$ Q-balls with positive parity are plotted as functions of the compact radial variable $x = \frac{r/r_0}{1 + r/r_0}$ at $r_0 = 6$, $\theta = \pi/2$ for some set of values of angular frequency ω at $m = 1$ and $\mu^2 = 0.25$ (upper plots) and $\mu^2 = 0$ (bottom plots).

with even and odd parity. The corresponding energy density distribution forms one or more tori, respectively. Similar to the spherically symmetric configuration with $n = 0$, the spinning Q-balls exist for all range of values of the angular frequency $\omega \in [0, 1]$. The limit of small Q-balls corresponds to the ω approaching the upper critical value, given by the mass of the complex component, in the opposite limit of small value of angular frequencies, spinning Q-ball rapidly expands.

We observe that, similar to the spinning Q-balls in the single component model [16, 17] for each value of integer winding number n , there are two types of solutions possessing different parity, so called parity-even and parity-odd Q-balls. Indeed, the equations (14) in

the limiting case of $\omega^2 \sim m^2$ (small Q-balls) can be linearized. Then the second of these equations is reduced to the standard harmonic equation and the solution are associated with the usual spherical harmonics

$$Y_l^n(\theta, \varphi) = \sqrt{\frac{2l+1}{4\pi} \frac{(l-n)!}{(l+n)!}} P_l^n(\cos \theta) e^{in\varphi}.$$

Here $P_l^n(\cos \theta)$ are the associated Legendre polynomials of degree l and order n . Thus, the spherically symmetric fundamental Friedberg-Lee-Sirlin Q-ball corresponds to the spherical harmonic Y_0^0 , and there are two spinning configuration in the sector $n = 1$, the parity-even solution Y_1^1 and parity-odd solution Y_2^1 , respectively. Further, this observation suggests that the equations (14) also support solutions which correspond to higher energy angular excitations of the fundamental Q-ball [19].

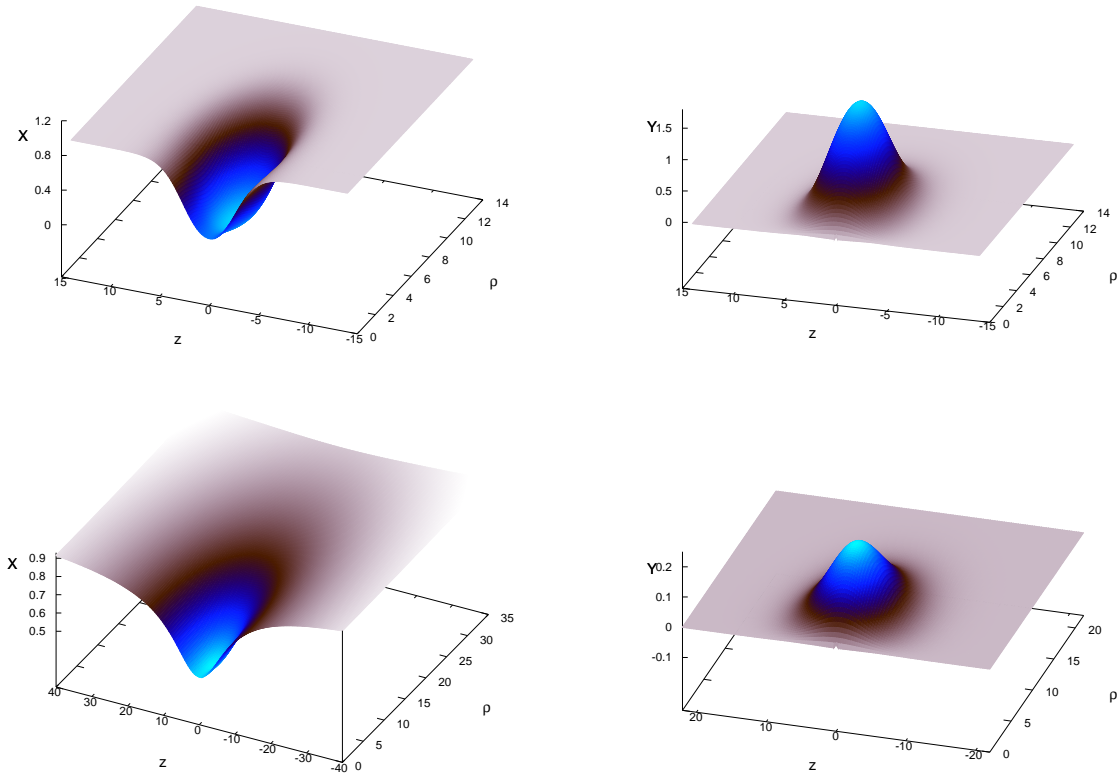


FIG. 6: The field components of the spinning $n = 1$ parity-even Q-ball at $\omega = 0.65$, $m = 1$, $\mu^2 = 0.25$ (upper row) and $\mu^2 = 0$ (bottom row) are shown as functions of the coordinates $\rho = \sin \theta$ and $z = r \cos \theta$.

In Figs. 6,7 we displayed the fields of the spinning parity-even and parity-odd Q-balls,

both in the massive and massless cases. For parity-even solutions the spinning component $Y(r, \theta)$ is maximal in the symmetry plane, as $\mu = 0$ the massless component $X(r, \theta)$ is minimal at the origin, it decays asymptotically, according to (10) (see Fig. 6, bottom left plot). If the mass of the $X(r, \theta)$ component is non-zero, it decays exponentially, as it is seen in Fig 6, upper left plot. We also observe that in the latter case the minimum of this component is shifted to the $x - y$ plane. The energy density distributions of the rotating even-parity Q-balls is torus-shaped in both cases. However, as the component $X(r, \theta)$ is massive, for the same value of the frequency ω , both the energy and the amplitudes of the fields are much larger.

Fig. 5 exhibits the profiles of the corresponding positive parity solutions in the symmetry plane $\theta = \pi/2$ at $m = 1$, $\mu^2 = 0.25$ and for $\mu = 0$ for some set of values of the angular frequency ω .

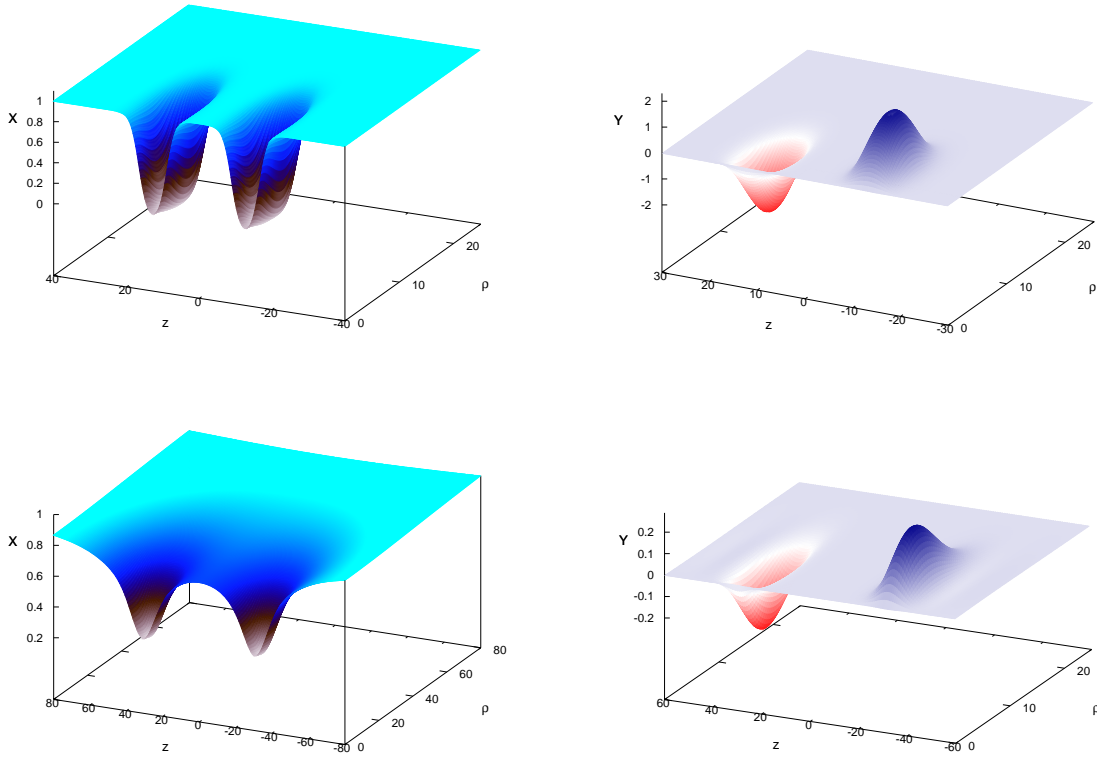


FIG. 7: The field components of the spinning $n = 1$ parity-odd Q-ball at $\omega = 0.50$, $m = 1$, $\mu^2 = 0.25$ (upper row) and $\mu^2 = 0$ (bottom row) are shown as functions of the coordinates $\rho = \sin \theta$ and $z = r \cos \theta$.

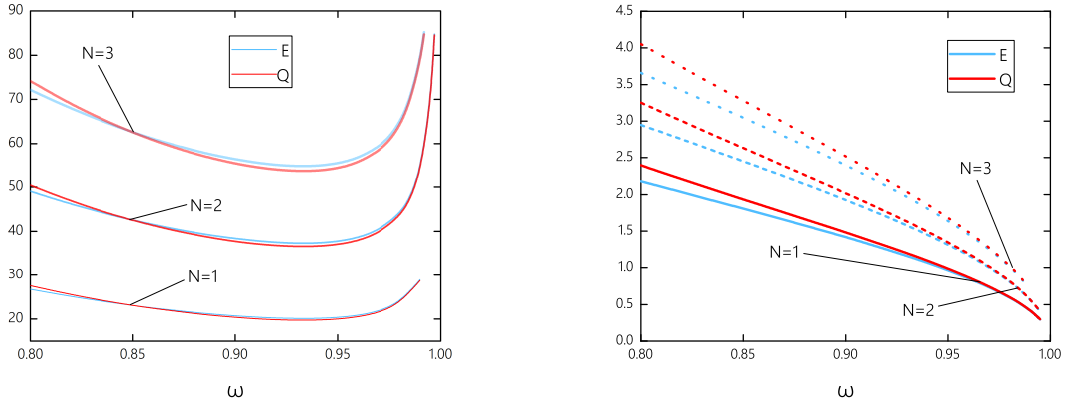


FIG. 8: The energy and the charge of the spinning parity-even Q-balls are shown in units of 8π as functions of the angular frequency ω at $m = 1$, $\mu^2 = 0.25$ (left) and $\mu^2 = 0$ (right).

The field components of the parity-odd $n = 1$ Q-ball are presented in Fig. 7. For this solutions the spinning component $Y(r, \theta)$ vanishes in the equatorial plane while the real field $X(r, \theta)$ possess two minima, located symmetrically with respect to the $x - y$ plane. The difference between the massive and massless cases is that, as $\mu = 0$, the field $X(r, \theta)$ decays asymptotically as $\sim 1/r$. Further, in such a case the minima of this component are located on the z -axis, see Fig. 7, bottom left plot. The energy density distribution of the parity-odd Q-balls has a double torus structure. Note that as the real component $X(r, \theta)$ becomes massless, the characteristic size of the configuration grows, the tori are well separated from each other.

Considering the frequency dependence of rotating Q-balls, we found that it is qualitatively the same as in the case of the fundamental $n = 0$ solutions, see Figs. 2,3 above.

In Fig. 8, left plot, we show the charge and the energy of the parity-even Q-balls as functions of the angular frequency ω . We observe that the solutions exist for all allowed range of values of ω restricted from above by the mass of the complex field $m = 1$. As ω approaches this upper limit, the amplitude of both components is decreasing. As the real component $X(r, \theta)$ remains massive, it decays exponentially. In such a case we observe the same usual pattern as in the model with single component complex field and a polynomial self-interaction potential [16, 17]. Both the energy and the charge of the configuration of these Q-balls are minimal at some critical value ω_{cr} and the curve $E(Q)$ shows the same cusp structure as displayed in Fig. 3, left plot. Thus, there are two branches of $E(Q)$ curves,

the existence of two different solutions with the same value of charge Q indicates that the more energetic configurations on the upper branch are unstable.

The situation is different for the spinning Q-balls with massless long-range component $X(r, \theta)$. As for the spherically symmetric $n = 0$ configurations, both the charge and the energy monotonically depend on ω , see Fig. 3, right plot. Thus, there is no critical frequency and only one branch of classically stable solutions exist for all range of values of ω . The scalar charge C of the spinning Q-balls with massless hair also depends on the angular frequency. Numerical calculations show that dependency of its value per rotational quantum number n is identical with the dependency of the scalar charge of the spherically symmetric hairy Q-ball displayed in Fig. 4 above.

IV. CONCLUSIONS

The objective of this work was to investigate properties of new Q-ball solutions with long-range massless scalar hair, existence of which was conjectured in the pioneering study [15].

As the real scalar component of the Friedberg-Lee-Sirlin Q-ball remains massive, these solutions exhibit the same general pattern as the corresponding non-topological solitons in the non-renormalizable model with polynomial potential. The solutions exist only in a finite frequency range, which is restricted from above by the value of the mass of the complex component. We also found that there are spinning generalizations of the fundamental spherically symmetric Friedberg-Lee-Sirlin Q-ball with both even and odd parity. The large Q-balls correspond to the small values of the angular frequency, they tend to the corresponding states of the perturbative spectrum as ω approaches the upper limiting value.

However, this pattern drastically changes, as the potential is vanishing. The vacuum expectation value of the real massless scalar field still remains non zero, this component possess long range Coulomb asymptotic tail. Such a hairy Q-ball has an additional scalar charge C , which corresponds to the weak long-range attractive interaction between the solitons. On the other hand, there is a short-range Yukawa interaction mediated by the complex component of the Friedberg-Lee-Sirlin Q-ball. If the interacting Q-balls are in phase, this interaction is attractive, while if they are out-of-phase it is repulsive, thus the resulting pattern of interaction between the Q-balls is rather complicated.

We found that the branch structure of the hairy Q-balls is different from the case when the real component remains massive. Notably, both the energy and the charge of the configuration decreases monotonically as ω increases. There is no second unstable branch of solutions, the hairy Q-balls with long-range real scalar component are classically stable within all range of values of the angular frequency.

The work here should be taken further by considering gauged spinning Q-balls with massless real scalar component, another interesting direction is to investigate properties of self-gravitating spinning Q-balls without potential. We hope we can address these issues in our future work.

Acknowledgements

Y.S. gratefully acknowledges support from the Ministry of Education and Science of Russian Federation, project No 3.1386.2017. He would like to thank the Department of Physics, Tokyo University of Science, for its kind hospitality.

-
- [1] R. Friedberg, T.D. Lee and A. Sirlin, Phys. Rev. D **13** (1976) 2739.
 - [2] S.R. Coleman, Nucl. Phys. B **262** (1985) 263; Erratum: Nucl. Phys. B **269** (1986) 744
 - [3] R. Friedberg, T. D. Lee and Y. Pang, Phys. Rev. D **35** (1987) 3658.
 - [4] P. Jetzer, Phys. Rept. **220** (1992) 163.
 - [5] T. D. Lee, Phys. Rev. D **35** (1987) 3637.
 - [6] A. Kusenko, Phys. Lett. B **405** (1997) 108.
 - [7] I. Affleck and M. Dine, Nucl. Phys. B **249** (1985) 361.
 - [8] A. Kusenko and M. E. Shaposhnikov, Phys. Lett. B **418** (1998) 46.
 - [9] K. N. Anagnostopoulos, M. Axenides, E. G. Floratos and N. Tetradis, Phys. Rev. D **64** (2001) 125006.
 - [10] K.M. Lee, J.A. Stein-Schabes, R. Watkins and L.M. Widrow, Phys. Rev. D **39** (1989) 1665.
 - [11] A. Kusenko, M.E. Shaposhnikov and P.G. Tinyakov, Pisma Zh. Eksp. Teor. Fiz. **67** (1998) 229; [JETP Lett. **67**, 247 (1998)]
 - [12] A. M. Safian, S.R. Coleman and M. Axenides, Nucl. Phys. B **297** (1988) 498.

- [13] K. Enqvist and M. Laine, JCAP 0308 (2003) 003.
- [14] Yu.M. Bunkov and G.E. Volovik, Phys. Rev. Lett. **98** (2007) 265302.
- [15] A. Levin and V. Rubakov, Mod. Phys. Lett. A **26** (2011) 409.
- [16] M.S. Volkov and E. Wohnert, Phys. Rev. D **66** (2002) 085003.
- [17] B. Kleihaus, J. Kunz and M. List, Phys. Rev. D **72** (2005) 064002 .
- [18] E. Radu and M.S. Volkov, Phys. Rept. **468** (2008) 101.
- [19] Y. Brihaye and B. Hartmann, Nonlinearity **21** (2008) 1937.
- [20] Y.M. Shnir, *Topological and Non-Topological Solitons in Scalar Field Theories*, (Cambridge University Press, Cambridge, 2018)
- [21] W. Schönauer and R. Weiß, "Efficient vectorizable PDE solvers" J. Comput. Appl. Math. 1989. V. 27. P. 279
M. Schauder, R. Weiß and W. Schönauer, "The CADSOL Program Package", Universität Karlsruhe, 1992. Interner Bericht Nr. 46/92.